Sensitivity calculations in PDF modelling of turbulent flames

Zhuyin Ren [*], Stephen B. Pope

Sibley School of Mechanical and Aerospace Engineering, Cornell University, Rhodes Hall 101, Ithaca, NY 14853, USA

Abstract

In modelling turbulent combustion, it is desirable to know the sensitivities of the predictions to certain parameters. Recently, a method for calculating particle-level sensitivities in PDF modelling of turbulent combustion has been described by Ren and Pope [1]. In this work, we develop a methodology for the efficient calculation of these particle-level sensitivities using *in situ* adaptive tabulation. In addition, PDF calculations with sensitivities of the Cabra H_2/N_2 jet flame are performed to investigate the sensitivities of the predictions to certain important parameters. The accuracy of the proposed methodology is demonstrated by comparing its prediction of sensitivities with those obtained by divided difference. For the Cabra flame, the sensitivities confirm that the predictions are extremely sensitive to the coflow temperature: the sensitivities to coflow temperature are about 10 times larger than those to chemistry, and about 100 times larger than those to the mixing model constant. The particle-level sensitivities show that, at the flame base, strong chemical reactions start at in very fuel-lean region, which indicates that this region is important to the stabilization of the flame. The sensitivities also indicate the physical regions where the effects of different parameters are significant. Further insights are obtained by investigating the compositions and the sensitivity vectors in the composition space. The most sensitive particles are found to lie close to a saddle-shaped two-dimensional manifold, and the sensitivity vectors are generally tangential to the manifold. The singular value decomposition of the sensitivity matrices reveals that there is only one significant singular value and hence there is a dominant direction of the response to a change in the sensitivity parameters considered. Similarities in particle sensitivities are also illustrated. Similar PDF calculations (with sensitivities) of the Barlow and Frank flame F are reported in the Supplementary material.
© 2009 The Combustion Institute. Published by Elsevier Inc. All rights reserved.

Keywords: Sensitivity analysis; *In situ* adaptive tabulation; Particle-level sensitivities; Local extinction/re-ignition; PDF methods

1. Introduction

Modelling combustion phenomena requires the knowledge of chemical kinetics, transport properties, turbulence/combustion model parameters, etc. as input parameters, and produces predictions (such as species concentration profiles, etc.) as the output, with the input and the output being connected by the governing model equations. Often it is desirable to know how sensitive the predictions are to certain parameters in the model formulation. In the fields of chemical kinetics and laminar flames, sensitivity analysis [2–4] has been widely used to examine quantitatively

* Corresponding author. Address: ANSYS Inc., 10 Cavendish Court, Lebanon, NH 03766, USA. Fax: +1 603 643 3967.
  E-mail address: zr26@cornell.edu (Z. Ren).

the relationship between the parameters and the output of the model. In contrast, sensitivity analysis in turbulent combustion calculations is less well developed. For example, in the past, in modelling turbulent reactive flows based on PDF methods [5], somewhat crude global sensitivity analyses have been performed by repeating a calculation with a single parameter changed by a small amount. This divided difference technique has been used to show the strong sensitivity of some PDF calculations of turbulent flames to the temperature of a pilot stream [6,7], to a reaction rate [8], and to the mixing model constant C_ϕ governing the rate of turbulent mixing [6,9–11]. However, using divided differences in PDF particle methods is costly and inefficient, as the statistical errors need to be reduced so as to be small compared to the differences in the two calculations.

Recently, Ren and Pope [1] developed a method for the accurate calculation of sensitivities in PDF modelling of turbulent combustion. It enables the calculation of sensitivities (to model parameters of interest) for each particle in the PDF particle method. These particle-level sensitivities are revealing: they allow one to examine the particles with the largest sensitivities, and the corresponding compositions reveal the sensitive regions in the composition and physical spaces. Moreover, sensitivities of mean (and conditional mean) quantities can be extracted by ensemble averaging the particle sensitivities.

A significant contribution of the present work is the development of a methodology for the efficient calculation of these particle-level sensitivities via the *in situ* adaptive tabulation (ISAT) algorithm [12]. In addition, PDF calculations with sensitivities of a lifted turbulent jet flame issuing into a vitiated co-flow stream (referred to as the Cabra flame) [13] are performed to investigate the sensitivities of the predictions to some important parameters.

The outline of the remainder of the paper is as follows. In Section 2, the new methodology for the calculation of sensitivities via ISAT in PDF particle methods is outlined. In Section 3, PDF calculations with sensitivities of the Cabra flame are described. Results are discussed in Section 4, and conclusions are drawn in Section 5. PDF calculations with sensitivities have also been performed for the Barlow and Frank flame F [14]. Because of space limitations, the description and results of these calculations are relegated to the Supplementary material.

2. Calculation of sensitivities in PDF particle methods via ISAT

In this section, we first briefly outline the formulation for sensitivity calculations in PDF parti-

cle methods (full details are in [1]). Then we elaborate on how ISAT is extended for the efficient calculation of sensitivities.

2.1. Formulation

In a PDF calculation of a reactive flow involving n_s species, the modelled PDF transport equation is usually solved numerically by a Lagrangian particle method, where the distribution of compositions is represented by an ensemble of particles. The composition $\phi^{(n)}$ of the nth particle consists of the n_s species specific moles and the sensible enthalpy, i.e., $n_\phi = n_s + 1$ quantities. In the PDF calculation, the change in particle composition due to reaction is treated exactly, while molecular mixing is modelled by a mixing model. In previous studies [15,11], the performance of different mixing models [16–20] has been examined: here the model used is the interaction by exchange with the mean (IEM or LMSE) model [16,17].

We consider a set $\mathbf{a} = \{a_1, a_2, \ldots, a_{n_a}\}$ of n_a sensitivity parameters. These could be: the temperature or species concentrations of an inflowing stream; the pre-exponential factor or the activation energy of a reaction; or the mixing model constant. In a fuller notation, $\phi_i^{(n)}(t; \mathbf{a})$ denotes the ith composition of the nth particle at time t for a PDF calculation performed with the sensitivity parameters having the values $\mathbf{a}$. The $n_\phi \times n_a$ sensitivity matrix $\mathbf{W}^{(n)}(t; \mathbf{a})$ (for the nth particle at time t) is defined by

$$W_{ij}^{(n)}(t; \mathbf{a}) \equiv \frac{\partial \phi_i^{(n)}(t; \mathbf{a})}{\partial a_j}. \tag{1}$$

In general, the evolution equation for $\phi^{(n)}(t; \mathbf{a})$ is given by

$$\frac{d\phi_i^{(n)}(t; \mathbf{a})}{dt} = S_i(\phi^{(n)}(t; \mathbf{a}); \mathbf{a}) + C_\phi M^{(n)}(\{\phi_i(t; \mathbf{a})\}), \tag{2}$$

where $\mathbf{S}$ is the rate of change due to chemical reactions, C_ϕ is the mixing model constant, and $M^{(n)}$ denotes the effect of the mixing model, which depends on the ensemble $\{\phi\}$ of particle compositions. Differentiating Eq. (2) with respect to a_j, we obtain the following evolution equation for the sensitivities $\mathbf{W}^{(n)}(t; \mathbf{a})$

$$\frac{dW_{ij}^{(n)}}{dt} = J_{ik}^{(n)} W_{kj}^{(n)} + V_{ij}^{(n)} + C_\phi M^{(n)}(\{W_{ij}\})$$
$$+ \frac{\partial C_\phi}{\partial a_j} M^{(n)}(\{\phi_i\}), \tag{3}$$

where the summation convention applies, $\mathbf{J}^{(n)}$ is the $n_\phi \times n_\phi$ Jacobian matrix $J_{ij} \equiv \partial S_i(\phi; \mathbf{a})/\partial \phi_j$, and we define $V_{ij} \equiv \partial S_i(\phi; \mathbf{a})/\partial a_j$ (the matrices $\mathbf{J}$ and $\mathbf{V}$ are accurately and efficiently evaluated

using automatic differentiation, e.g., by using ADIFOR [21]). In Eq. (3), the last two terms represent the effect of the mixing on particle sensitivities, which depend on the ensemble $\{\phi\}$ of particle compositions and the ensemble $\{\mathbf{W}\}$ of particle sensitivities, respectively. As discussed in [1], the derivation of Eq. (3) from Eq. (2) neglects the secondary effects arising from the dependence of density on the sensitivity parameters.

In the computational implementation, for the nth particle, the sensitivity matrix $\mathbf{W}^{(n)}$ is represented in addition to the composition $\phi^{(n)}$. The particle properties $\phi^{(n)}(t)$ and $\mathbf{W}^{(n)}(t)$ then evolve by Eqs. (2) and (3) with appropriate initial and boundary conditions. For example, if a_j is a model parameter, then the appropriate boundary condition is $W_{ij} = 0$ for all i. If a_j corresponds to ϕ_i on the boundary considered, then the boundary conditions are $W_{ij} = 1$ for $i = j$ and $W_{ij} = 0$ for $i \neq j$.

As shown in [1], Eqs. (2) and (3) can be accurately solved using splitting schemes, where the reaction terms and transport terms are separated into different sub-steps. In the transport sub-step, the system solved is

$$\frac{d\phi_i^{(n)}}{dt} = C_\phi M^{(n)}(\{\phi_i\}),$$
$$\frac{dW_{ij}^{(n)}}{dt} = C_\phi M^{(n)}(\{W_{ij}\}) + \frac{\partial C_\phi}{\partial a_j} M^{(n)}(\{\phi_i\}). \quad (4)$$

If the mixing model constant C_ϕ is not included as one of the sensitivity parameters, then $\partial C_\phi / \partial a_j$ is zero (for all j) and the last term in the sensitivity equation is absent. For this case, the system is solved simply by applying the mixing model to each component of the particle composition and the particle sensitivities over a time step. The legitimacy of this simple procedure stems from the linearity of the mixing operation. Otherwise, if C_ϕ is one of the sensitivity parameters, the particle compositions and the particle sensitivities to other sensitivity parameters except C_ϕ are still obtained simply by applying the mixing model to each component of them over a time step. A second-order accurate solution to the sensitivities to C_ϕ can be obtained based on a three-step procedure as shown in [1].

During the reaction sub-step, the reaction source terms are integrated, corresponding to the equations (written in a simplified matrix notation, omitting the particle index, n)

$$\frac{d\phi}{dt} = \mathbf{S}(\phi), \quad (5)$$
$$\frac{d\mathbf{W}}{dt} = \mathbf{J}(\phi)\mathbf{W} + \mathbf{V}(\phi). \quad (6)$$

In [1], Eqs. (5) and (6) are integrated using the ODE solver DDASAC [22]. This direct integration for each particle on each time step is computationally inefficient and costly. In this study, the efficient solution for Eqs. (5) and (6) is achieved via ISAT.

2.2. Efficient solution to the reaction sub-step via ISAT

In PDF calculations without sensitivities, the governing equation for the reaction sub-step is Eq. (5). Given the initial composition $\phi^0 \equiv \phi(t_0)$ at time t_0, the reaction mapping $\mathbf{R}(\phi^0) \equiv \phi(t_0 + \Delta t)$ after a time step Δt can be efficiently computed by the ISAT algorithm (recall that Eq. (5) is autonomous: with a fixed time step Δt, $\mathbf{R}(\phi^0)$ depends only on ϕ^0). That is, the composition $\mathbf{R}(\phi^0)$ at the end of the time step is tabulated as a function of the initial composition ϕ^0. Table entries are added as needed (for possible later use) by using the ODE integrator DDASAC, to solve Eq. (5) for $\mathbf{R}(\phi^0)$, in conjunction with the equation

$$\frac{d\mathbf{A}(t)}{dt} = \mathbf{J}(\phi(t))\mathbf{A}(t), \quad (7)$$

from the initial condition $\mathbf{A}(t_0) = \mathbf{I}$ to obtain the $n_\phi \times n_\phi$ dimensional sensitivity matrix (with respect to the initial composition) $\widehat{\mathbf{A}}(\phi^0) \equiv \mathbf{A}(t_0 + \Delta t)$, which (as denoted) depends only on ϕ^0 (for fixed Δt) (note that $\mathbf{A}$ and $\mathbf{W}$ are completely different sensitivity matrices: $\mathbf{A}$ is with respect to compositions ϕ^0 at the beginning of a time step; $\mathbf{W}$ is with respect to the specified sensitivity parameters, $\mathbf{a}$). The matrix $\widehat{\mathbf{A}}(\phi^0)$ is also stored in the ISAT table and is used in the construction of a linear approximation for $\mathbf{R}(\phi)$. That is, for a given query composition ϕ^q close to the tabulated point ϕ^0, a linear approximation to $\mathbf{R}(\phi^q)$, denoted as $\mathbf{R}^l(\phi^q)$, is obtained as

$$\mathbf{R}^l(\phi^q) \equiv \mathbf{R}(\phi^0) + \widehat{\mathbf{A}}(\phi^0)(\phi^q - \phi^0). \quad (8)$$

When ISAT is employed for both the composition and sensitivity calculations, the following observations are made. The solution to Eq. (6), $\mathbf{W}(t)$, can be written as

$$\mathbf{W}(t) = \overline{\mathbf{W}}(t) + \mathbf{A}(t)\mathbf{W}^0, \quad (9)$$

where $\mathbf{W}^0 \equiv \mathbf{W}(t_0)$ is the initial condition, and $\overline{\mathbf{W}}(t)$ is the solution to Eq. (6) from the initial condition $\overline{\mathbf{W}}(t_0) = 0$. Note that, for given Δt, the solution $\overline{\mathbf{W}}(t_0 + \Delta t)$ depends solely on the initial condition ϕ^0, and hence we can define $\widehat{\mathbf{W}}(\phi^0)$ to be this solution, i.e., $\widehat{\mathbf{W}}(\phi^0) = \overline{\mathbf{W}}(t_0 + \Delta t)$. Hence the sensitivity matrix after a time step Δt is

$$\mathbf{W}(t_0 + \Delta t) = \overline{\mathbf{W}}(t_0 + \Delta t) + \mathbf{A}(t_0 + \Delta t)\mathbf{W}^0$$
$$= \widehat{\mathbf{W}}(\phi^0) + \widehat{\mathbf{A}}(\phi^0)\mathbf{W}^0. \quad (10)$$

The basis of the current implementation is to use ISAT to tabulate $\widehat{\mathbf{W}}(\phi^0)$ (in addition to $\mathbf{R}(\phi^0)$ and $\widehat{\mathbf{A}}(\phi^0)$) so that $\mathbf{W}(t_0 + \Delta t)$ can be efficiently evaluated by Eq. (10), thus avoiding the expensive

integration of Eq. (6). As now explained, only part of $\widehat{\mathbf{W}}(\phi^0)$ needs to be tabulated.

The sensitivity parameters **a** can be partitioned into two groups $\{\mathbf{a}_1, \mathbf{a}_2\}$, having n_{a1} and n_{a2} components, respectively. By definition, the parameters in group $\mathbf{a}_1$ do not affect the reaction source term (i.e., $V_{ij} = \partial S_i / \partial a_j = 0$), and may correspond to boundary conditions or the mixing model constant; whereas the parameters in group $\mathbf{a}_2$ are pre-exponential factors (or other parameters) in reaction rates. Correspondingly, the sensitivity matrix **W** can be partitioned as $\{\mathbf{W}_1, \mathbf{W}_2\}$ with $\mathbf{W}_1$ and $\mathbf{W}_2$ being the sensitivities to the parameters in group $\mathbf{a}_1$ and $\mathbf{a}_2$, respectively. For parameters in group $\mathbf{a}_1$, one has the trivial solution $\widehat{\mathbf{W}}_1(\phi^0) = 0$ (since $\mathbf{V}_1 = 0$) and the corresponding sensitivities after the reaction sub-step are simply $\mathbf{W}_1(t_0 + \Delta t) = \widehat{\mathbf{A}}(\phi^0)\mathbf{W}_1^0$. Only for parameters in group $\mathbf{a}_2$, do the corresponding components of Eq. (6) need to be integrated to obtain $\widehat{\mathbf{W}}_2(\phi^0)$. Then the sensitivities after reaction are obtained using Eq. (10), i.e., $\mathbf{W}_2(t_0 + \Delta t) = \widehat{\mathbf{W}}_2(\phi^0) + \widehat{\mathbf{A}}(\phi^0)\mathbf{W}_2^0$.

When an entry is added to the ISAT table, in addition to ϕ, $\mathbf{R}(\phi)$ and $\widehat{\mathbf{A}}(\phi)$, the non-trivial $\widehat{\mathbf{W}}_2(\phi)$ is also computed using DDASAC and stored in the table. For a new query point, if the composition ϕ^q is close to a tabulated point ϕ, a linear approximation to $\mathbf{R}(\phi^q)$ is obtained via Eq. (8). Moreover, constant approximations to $\widehat{\mathbf{A}}(\phi^q)$ and $\widehat{\mathbf{W}}_2(\phi^q)$ are obtained as $\widehat{\mathbf{A}}(\phi^q) \approx \widehat{\mathbf{A}}(\phi)$ and $\widehat{\mathbf{W}}_2(\phi^q) \approx \widehat{\mathbf{W}}_2(\phi)$. Then the sensitivities after reaction for the query point are obtained using Eq. (10) (with $\widehat{\mathbf{W}}_1 = 0$).

In this study, the most recent ISAT implementation, ISAT5 [23] has been extended to enable sensitivity calculations. In the implementation, ISAT explicitly controls the approximation errors in compositions by a user specified error tolerance, whereas for the sensitivities, there is no explicit error control. By performing an accuracy study, we find that the error control in compositions is sufficient to guarantee the accuracy of the sensitivities.

2.3. Computational considerations

In PDF particle computations with sensitivities, for each particle the sensitivity matrix **W** is represented in addition to the composition, which results in an increase in particle storage requirements of a factor of n_a. However, as far as the storage for ISAT is concerned, the only additional quantity that needs to be stored for each table entry is the $n_\phi \times n_{a2}$ matrix $\widehat{\mathbf{W}}_2$ (recall that each table entry already involves the storage of several $n_\phi \times n_\phi$ matrices). If the sensitivity parameters consist entirely of group 1 parameters (i.e., ones of which the reaction rate is independent, such as boundary conditions and the mixing model constant), then there is no additional storage requirement for ISAT.

The additional computational work caused by the sensitivity calculations lies mainly in the mixing and reaction sub-steps. Mixing must be performed for the sensitivities as well as for the compositions. In the reaction sub-step, when adding new entries to the ISAT table, in addition to $\mathbf{R}(\phi)$, one needs to compute $\widehat{\mathbf{W}}_2(\phi)$; when retrieving from the ISAT table, the additional work is the matrix–matrix multiplication **AW**, which requires of order $n_a n_\phi^2$ operations—at most a factor n_a more than already required by ISAT for the linear approximation to $\mathbf{R}(\phi)$.

3. PDF calculations of the Cabra flame with sensitivities

This study, for the first time, investigates the sensitivities (including the particle-level sensitivities) in the PDF calculations of turbulent flames. The flame considered is the Cabra H_2/N_2 jet flame [13], which is a turbulent jet flame of H_2/N_2 issuing into a wide co-flow of lean combustion products and is designed to simulate conditions, albeit with simple flows, that are encountered in gas turbine combustors and furnaces where there is a recirculation of hot combustion products. Measurement shows that the liftoff height of this flame is very sensitive to the coflow temperature T_c, such that a decrease of 10 K in T_c can double the liftoff height. Comprehensive PDF model investigations of this flame, such as the issues of autoignition and flame stabilization as well as detailed comparison between numerical calculations and measurement, have been performed in [7,8,13,25,26]. In previous PDF calculations [7,8,13,25], crude sensitivities to the coflow temperature T_c, mixing model constant C_ϕ, as well as chemistry are obtained by repeating the calculation with a single parameter changed by a small amount.

The emphasis of this study is to investigate the sensitivities of the calculations to model parameters of interest and to gain new insights into the physical processes of the flame by interrogating the particle sensitivities. The PDF calculations are performed using the code HYB2D [27], which implements a hybrid finite-volume/particle algorithm and has been used in previous calculations such as [11,24,26]. Here, the HYB2D code has been extended to accommodate the sensitivity calculation (together with the extended ISAT algorithm).

In the PDF calculations, the Li mechanism [28] is employed with the ISAT error tolerance $\varepsilon_{tol} = 6.25 \times 10^{-6}$; the IEM mixing model is considered with $C_\phi = 1.5$; and radiative heat loss is neglected. The other details of the calculations are identical to those in [7,26]. By employing the method described in Section 2, here we compute the particle-level sensitivities to the mixing model constant C_ϕ, the coflow temperature T_c, and the

pre-exponential factors $\{\alpha_1; \alpha_2; \alpha_3\}$ of the three chain reactions: $R1 : O_2 + H \Longleftrightarrow OH + O$; $R2 : H_2 + O \Longleftrightarrow OH + H$; $R3 : H_2 + OH \Longleftrightarrow H_2O + H$, respectively, i.e., $\mathbf{a} = \{C_\phi; T_c; \alpha_1; \alpha_2; \alpha_3\}$.

To save computational time, a PDF calculation without sensitivities is first carried out until the statistically stationary state has been reached. Then the calculation with sensitivities is performed restarting from this computed statistically stationary state. The sensitivity calculation has no effect on the computed compositions or velocities, and so the statistically stationary state for these quantities is maintained.

4. Results

In this section, we investigate the sensitivities in the PDF calculations of the Cabra flame in terms of the dimensional semi-logarithmic sensitivities

$$\widetilde{W}_{ij}^{(n)}(t; \mathbf{a}) \equiv \frac{\partial \phi_i^{(n)}(t; \mathbf{a})}{\partial \ln a_j} = a_{(j)} W_{ij}^{(n)}(t; \mathbf{a}), \qquad (11)$$

where bracketed suffixes are excluded from the summation convention.

4.1. Mean sensitivities

In physical space (normalized by the jet diameter D), Fig. 1 shows the contour plots of the mean specific moles of OH and its semi-logarithmic sensitivities to C_ϕ, α_1 and T_c (the radical OH is used as the flame marker in previous studies [7,8,13,25]). The results are obtained by time averaging over 5000 time steps after the sensitivity calculations have reached a statistically stationary state. The sensitivities to α_2 and α_3 are qualitatively similar to the sensitivities to α_1, but smaller in magnitude (see Fig. S1 in the Supplementary material). Several important observations are as follows.

As revealed by the the sensitivities, the most sensitive parameter for this flame is the coflow temperature T_c. The calculation is extremely sensitive to T_c with the normalized sensitivity $(\partial \ln \tilde{z}_{OH} / \partial \ln T_c)$ being of order 100. The sensitivity to T_c is about 10 times larger than the sensitivity to α_1, and about 100 times larger than that to C_ϕ. For the mean of the species OH, the maximum sensitivity to α_1 and T_c occurs around the axial location $x/D = 9 - 10$ and radial location $r/D \approx 1$, whereas the maximum sensitivity to C_ϕ occurs around $x/D = 11.5 - 14.5$ and $r/D \approx 1$.

The sensitivities also indicate the physical region where the effects of different parameters are significant. For the mean of the species OH, the sensitivities to α_1 and to T_c are qualitatively similar in terms of their distribution in physical space, and the effect of α_1 and T_c are significant only in the range $7 < x/D < 15$. The sensitivities to α_1 and to T_c are different from the sensitivities to C_ϕ, particularly further downstream, away from the flame base. Away from the flame base, the flame is mixing controlled, and it is sensitive to the mixing model constant, but not to chemistry and the coflow temperature. Also the region of negative sensitivity for α_1 and T_c is different from that for C_ϕ.

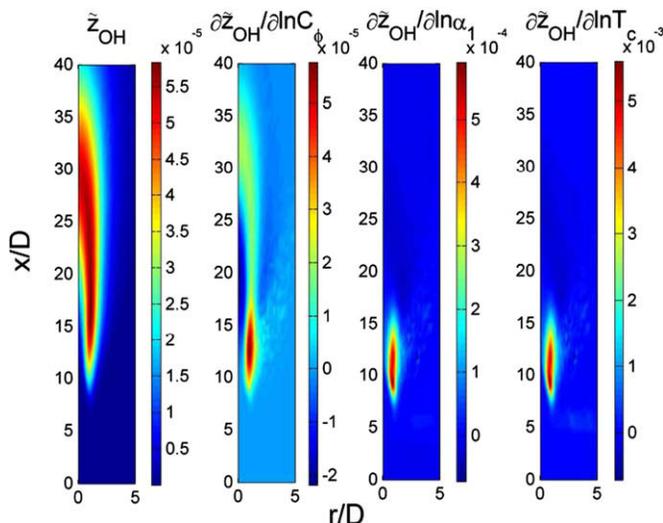Similar observation can also be made for other species such as H_2O (see Fig. S2).

Fig. 1. In physical space, contour plots of the mean specific moles of OH and its semi-logarithmic sensitivities to the mixing model constant C_ϕ, the pre-exponential factor α_1, and the coflow temperature T_c (note that in the four plots the upper limits of the color scales are approximately 5×10^{-5}, 5×10^{-5}, 5×10^{-4} and 5×10^{-3}, respectively).
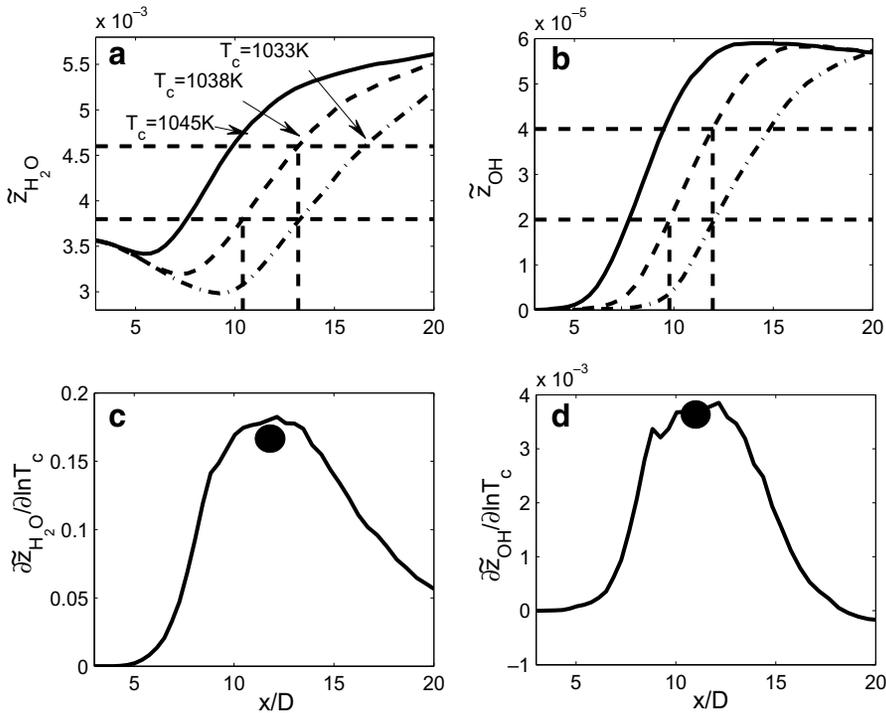
Fig. 2. At the radial location $r/D = 1.094$, figure showing (a) axial profiles of $\tilde{z}_{H_2O}$ for three co-flow temperatures; (b) axial profiles of $\tilde{z}_{OH}$; (c) solid line: profile of the mean sensitivity $\partial\tilde{z}_{H_2O}/\partial\ln T_c$ (extracted from particle sensitivities) with $T_c = 1038$ K, solid dot: the mean sensitivity obtained by divided difference (see Section 4.2) for $10.4 < x/D < 13.2$; (d) solid line: profile of the mean sensitivity $\partial\tilde{z}_{OH}/\partial\ln T_c$ (extracted from particle sensitivities) with $T_c = 1038$ K, solid dot: the mean sensitivity obtained by divided difference for $9.8 < x/D < 12$.

4.2. Accuracy

As a check on accuracy, we compare the mean sensitivities obtained by the present method with those obtained by repeating the calculation with a single parameter changed by a small amount. Specifically, the sensitivities to the coflow temperature T_c are compared.

Figure 2a and b show axial profiles of the mean species $\tilde{z}_{H_2O}$ and $\tilde{z}_{OH}$ at the radial location $r/D = 1.094$ (i.e., $r = 5$ mm) from the PDF calculations with three different coflow temperatures. As shown, with 12 K decrease in T_c (from 1045 K to 1033 K), the location x^* of $\tilde{z}_{H_2O} = 4 \times 10^{-3}$ kmol/kg shifts from about $x^*/D = 8$ to $x^*/D = 14$. Notice that in the region where $3.8 \times 10^{-3} < \tilde{z}_{H_2O} < 4.6 \times 10^{-3}$, the slopes of the H$_2$O profiles (with different coflow temperatures) do not vary significantly; and neither do the OH profiles in the region where $2 \times 10^{-5} < \tilde{z}_{OH} < 4 \times 10^{-5}$.

Figure 2c and d show the axial profiles of the mean sensitivities (extracted from particle sensitivities) $\partial\tilde{z}_{H_2O}/\partial\ln T_c$ and $\partial\tilde{z}_{OH}/\partial\ln T_c$ with $T_c = 1038$ K. Also shown are the results from the divided difference approximation, which computes the mean sensitivities in the region

$3.8 \times 10^{-3} < \tilde{z}_{H_2O} < 4.6 \times 10^{-3}$ (corresponding to $10.4 < x/D < 13.2$ for $T_c = 1038$ K) and $2 \times 10^{-5} < \tilde{z}_{OH} < 4 \times 10^{-5}$ (corresponding to $9.8 < x/D < 12$ for $T_c = 1038$ K). In these regions, the sensitivity of a mean species $\tilde{z}_i$ to T_c can be obtained as

$$\frac{d\tilde{z}_i}{dT_c} = \frac{d\tilde{z}_i}{d(x/D)}\frac{d(x^*/D)}{dT_c}, \tag{12}$$

where x^*/D is the axial location of this value of $\tilde{z}_i$. The $d(x^*/D)/dT_c$ term can be obtained via divided difference. Here, for H$_2$O, $d(x^*/D)/dT_c$ is obtained using $\tilde{z}_{H_2O} = 4.2 \times 10^{-3}$ on the profiles of $T_c = 1033$ K and $T_c = 1045$ K; for OH, $d(x^*/D)/dT_c$ is obtained using $\tilde{z}_{OH} = 3 \times 10^{-5}$ on the profiles of $T_c = 1033$ K and $T_c = 1045$ K. The term $d\tilde{z}_i/d(x/D)$ is the slope of the profiles at $\tilde{z}_i$. Here, $d\tilde{z}_{H_2O}/d(x/D)$ is evaluated at $\tilde{z}_{H_2O} = 4.2 \times 10^{-3}$ on the profile of $T_c = 1038$ K; $d\tilde{z}_{OH}/d(x/D)$ is evaluated at $\tilde{z}_{OH} = 3 \times 10^{-5}$ on the profile of $T_c = 1038$ K.

As may be seen, in the region $10.4 < x/D < 13.2$ for H$_2$O and $9.8 < x/D < 12$ for OH, the mean sensitivities (extracted from particle sensitivities) are close to a constant. The general agreement between the computed sensitivities and those estimated by divided differences provides

reassurance about the correctness of the implementation of the current method. It also suggests that in this case there is at most a small impact of the neglect of the secondary effects due to changes in density resulting from changes in the sensitivity parameters.

4.3. Particle sensitivities in the region of the flame base

Substantial efforts have been made to understand the stabilization mechanism of this flame. By considering some numerical indicators (developed to distinguish between of flame stabilization by auto-ignition as opposed to stabilization through partially premixed flame propagation), Gordon et al. [25] conclude that the Cabra flame is stabilized by the autoignition process. Also, Wang and Pope [26] recently shed new insights on this autoignition process through analyzing Lagrangian time series of particle properties from PDF calculations.

Here, we investigate this physical process by interrogating the particle sensitivities in the base region of the flame, which is taken to be $6 \leqslant x/D \leqslant 10$ and $0 < r/D < 2$. The N (with $N = 1200$) particles from this region with the largest sensitivities to α_1 (i.e., to chemistry) are examined in different spaces. (Large sensitivities to α_1 imply strong chemical reactions.) Specifically, we study the sensitivities in the x/D-ξ and T-ξ spaces, where ξ is mixture fraction and T is temperature.

Figure 3 shows the scatter plots of particle sensitivities with respect to the pre-exponential factor α_1 for species OH. (The scatter plots of particle sensitivities with respect to T_c [see Fig. S3] are qualitatively similar.) As shown in the $x/D - \xi$
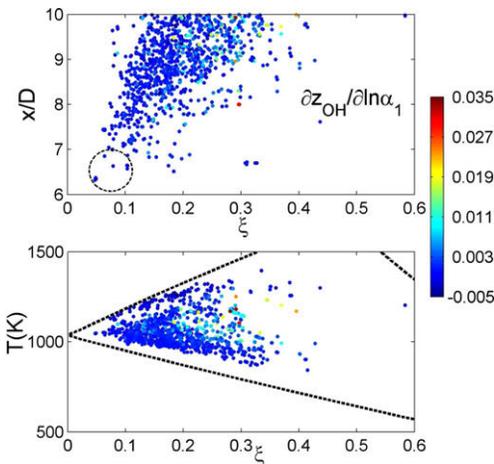

Fig. 3. Figure showing the scatter plot of the 1200 particles (with the largest sensitivities $\partial z_{OH}/\partial ln\alpha_1$, in magnitude) from the flame base in ξ-x space and ξ-T space, respectively. The dots are colored by $\partial z_{OH}/\partial ln\alpha_1$. The dashed lines in the lower plot are the equilibrium line and the mixing line.

plot, Fig. 3a, at the flame base, the mixture fraction of the first particle with large sensitivity is extremely small (about 0.05). (Recall the stoichiometric mixture fraction is 0.47 for this flame.) This implies that at the flame base, strong chemical reactions start at the very fuel-lean region. These ignition spots at the very fuel-lean region are significant for the flame stabilization. This is consistent with the findings in [26] that along the mixing line between the fuel composition and coflow composition, the shortest ignition delay times occur at the very fuel-lean region. For further downstream locations, large sensitivities propagate toward larger mixture fractions. Through the whole flame base region, for OH, the largest sensitivities are confined to the fuel-lean side, in the range $0.05 < \xi < 0.4$. Similar observation can be made for H_2O (see Fig. S4).

Further insights are obtained by investigating the sensitivity vector such as $\tilde{w}_{\alpha_1}$ in the composition space (as the name indicates, $\tilde{w}_{\alpha_1}$ denotes the sensitivity of ϕ with respect to the pre-exponential factor α_1). As may be seen from Fig. 4, the sensitivity vectors $\tilde{w}_{\alpha_1}$ appear to be in (or very close to) the tangent plane of a saddle-shaped manifold. To explain this figure: a principle component analysis is performed of the N species vectors z; these vectors are then transformed into the principle axes; and the dots in the figure are a scatter plot of the first three principle components. As may be seen, the dots lie close to a saddle-shaped two-dimensional manifold. Attached to each dot is a line segment in the direction of $\tilde{w}_{\alpha_1}$, and these generally are tangential to the manifold. Further study shows that $\tilde{w}_{\alpha_2}$, $\tilde{w}_{\alpha_3}$ and $\tilde{w}_{T_c}$ are in the same direction as $\tilde{w}_{\alpha_1}$, whereas $\tilde{w}_{C_\phi}$ may not be aligned with $\tilde{w}_{\alpha_1}$ (see Fig. S5).

More insights are obtained from the singular value decomposition (SVD) of the sensitivity matrices $\tilde{W}$, viz., $\tilde{W} = U \Sigma P^T$, where U and P are orthogonal matrices, and Σ is the diagonal matrix
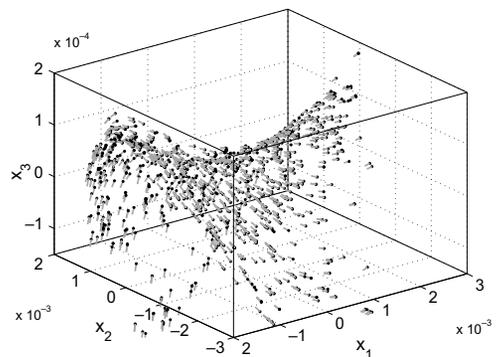

Fig. 4. In the subspace spanned by the first three principle axes, figure showing the scatter plot of the 1200 particles (with the largest sensitivities $\partial z_{OH}/\partial ln\alpha_1$, in magnitude) from the flame base. Attached to each dot is a line segment in the direction of the sensitivity $\partial z/\partial ln\alpha_1$.

of the singular values $\sigma_1 \geqslant \sigma_2 \geqslant \cdots \geqslant \sigma_{n_a} \geqslant 0$. From the SVD of $\tilde{\mathbf{W}}$ for the $N = 1200$ most sensitive particles, a striking observation is that there is only one significant singular value: the average and maximum values of σ_2/σ_1 are 6.4×10^{-4} and 0.032; and, if C_ϕ is omitted from the sensitivities, these ratios decrease to 4.2×10^{-5} and 9.8×10^{-4}.

Since only the first singular value is significant, the change $d\phi$ resulting from the infinitesimal change $d \ln \mathbf{a}$ can be written

$$d\phi = \tilde{\mathbf{W}}d \ln \mathbf{a} = \mathbf{u}\sigma_1\mathbf{p}^T d \ln \mathbf{a}, \qquad (13)$$

where the unit vectors $\mathbf{u}$ and $\mathbf{p}$ are the first columns of $\mathbf{U}$ and $\mathbf{P}$, respectively. Thus, in composition space, $\mathbf{u}$ is the direction of the response to a change in the parameters. The components u_j indicate the relative change in ϕ_j to $\ln \mathbf{a}$. The four largest components of $\mathbf{u}$ (in magnitude) correspond to H_2, O_2, H_2O and H. The components p_j indicate the relative sensitivities of ϕ to $\ln a_j$. The components of $\mathbf{p}$ corresponding to T_c, α_1, α_2 and α_3 vary little (in logarithmic scale) from particle to particles, with their values being 0.99, 0.11, 0.02, and 0.03 respectively. The component of $\mathbf{p}$ corresponding to C_ϕ exhibits more variation, with its minimum and maximum values (over the N samples) being 6×10^{-5} and 3×10^{-2}. More details are in Fig. S6.

Another consequence of only the first singular value being significant is the observed similarities in particle sensitivities. The first type of similarity is local similarity, where the ratio of the sensitivities of two variables with respect to the same parameter is equal (for any parameter of α_1, α_2, α_3, or T_c). The second type of similarity is global similarity, where the ratio of the sensitivities of any variable with respect to any two parameters (of α_1, α_2, α_3, or T_c) is equal. These similarities are illustrated in Fig. S7.

5. Conclusion

In this work, the efficient calculation of particle-level sensitivities in PDF modelling of turbulent combustion is achieved using *in situ* adaptive tabulation [12]. For the first time, PDF calculations of turbulent flames with particle sensitivities are performed to investigate the sensitivities of the predictions to model parameters of interest.

For the Cabra H_2/N_2 jet flame considered, as revealed by the the mean sensitivities, the calculations are extremely sensitive to the coflow temperature. The sensitivities to coflow temperature are about 10 times larger than those to chemistry, and 100 times larger than those to the mixing model constant. Moreover, the sensitivities to chemistry and coflow temperature are shown to

be qualitatively similar, but different from those to the mixing model constant. The sensitivity calculations also indicate the physical region where the effect of different parameters is significant. For the mean of the species OH, the effect of chemistry and coflow temperature persist only at the base of the flame, and it is insensitive to chemistry and the coflow temperature further downstream. The particle-level sensitivities of the Cabra flame shows that at the flame base, strong chemical reactions start at the very fuel-lean region, which indicates the very fuel-lean region is important for the flame stabilization.

Further insights are obtained by investigating the compositions and the sensitivity vectors in the composition space. As demonstrated, the most sensitive particles lie close to a saddle-shaped two-dimensional manifold and the sensitivity vectors (of parameters α_1, α_2, α_3, and T_c) are generally tangential to the manifold. The singular value decomposition of the sensitivity matrices reveals that there is only one significant singular value and hence there is a dominant direction of the response to a change in the sensitivity parameters considered. Similarities in particle sensitivities are also illustrated.

Similar PDF calculations (with sensitivities) of the Barlow and Frank flame F are reported in the Supplementary material.

Appendix A. Supplementary data

Supplementary data associated with this article can be found, in the online version, at doi:10.1016/j.proci.2008.05.074.

References

[1] Z. Ren, S.B. Pope, *Combust. Flame* 153 (2008) 202–215.
[2] H. Rabitz, M. Kramer, D. Dacol, *Ann. Rev. Phys. Chem.* 34 (1983) 419–461.
[3] T. Turányi, *J. Math. Chem.* 5 (1990) 203–248.

[4] A.E. Lutz, R.J. Kee, J.A. Miller, *SENKIN: A Fortran program for predicting homogeneous gas phase chemical kinetics with sensitivity analysis*, Technical Report SAND87-8248, Sandia National Laboratories, 1987.

[5] S.B. Pope, *Prog. Energy Combust. Sci.* 11 (1985) 119–192.

[6] Q. Tang, J. Xu, S.B. Pope, *Proc. Combust. Inst.* 28 (2000) 133–139.

[7] R. Cao, S.B. Pope, A.R. Masri, *Combust. Flame* 142 (2005) 438–453.

[8] A.R. Masri, R. Cao, S.B. Pope, G.M. Goldin, *Combust. Theory Model.* 8 (2004) 1–22.

[9] J. Xu, S.B. Pope, *Combust. Flame* 123 (2000) 281–307.

[10] R.P. Lindstedt, S.A. Louloudi, E.M. Váos, *Proc. Combust. Inst.* 28 (2000) 149–156.

[11] R. Cao, H. Wang, S.B. Pope, *Proc. Combust. Inst.* 31 (2007) 1543–1550.

[12] S.B. Pope, *Combust. Theory Model.* 1 (1997) 41–63.

[13] R. Cabra, T. Myrvold, J.Y. Chen, R.W. Dibble, A.N. Karpetis, R.S. Barlow, *Proc. Combust. Inst.* 29 (2002) 1881–1888.

[14] R.S. Barlow, J.H. Frank, *Proc. Combust. Inst.* 27 (1998) 1087–1095.

[15] Z. Ren, S.B. Pope, *Combust. Flame* 136 (2004) 208–216.

[16] J. Villermaux, J.C. Devillon, *in: Proceedings of the Second International Symposium on Chemical Reaction Engineering*, Elsevier, New York, 1972.

[17] C. Dopazo, E.E. O'Brien, *Acta Astronaut.* 1 (1974) 1239–1266.

[18] J. Janicka, W. Kolbe, W. Kollman, *J. Nonequilib. Thermodyn.* 4 (1979) 47–66.

[19] P.A. Nooren, H.A. Wouters, T.W.J. Peeters, D. Roekaerts, U. Maas, D. Schmidt, *Combust. Theory Model.* 1 (1997) 79–96.

[20] S. Subramaniam, S.B. Pope, *Combust. Flame* 115 (1998) 487–514.

[21] ADIFOR 2.0, Automatic Differentiation of Fortran, Available from: <http://www-unix.mcs.anl.gov/autodiff/ADIFOR/>.

[22] M. Caracotsios, W.E. Stewart, *Comput. Chem. Eng.* 9 (4) (1985) 359–365.

[23] L. Lu, S.B. Pope, *J. Comput. Phys.*, doi:10.1016/j.jcp.2008.09.015.

[24] R. Cao, S.B. Pope, *Combust. Flame* 143 (2005) 450–470.

[25] R.L. Gordon, A.R. Masri, S.B. Pope, G.M. Goldin, *Combust. Theory Model.* 11 (2007) 351–376.

[26] H. Wang, S.B. Pope, Lagrangian investigation of local extinction, re-ignition and auto-ignition in turbulent flames, *Combust. Theory Model.*, in press.

[27] M. Muradoglu, S.B. Pope, D.A. Caughey, *J. Comput. Phys.* 172 (2001) 841–878.

[28] J. Li, Z. Zhao, A. Kazakov, F.L. Dryer, *Int. J. Chem. Kin.* 36 (2004) 566–575.